

Test of first-principle calculations of charge transfer and electron-hole distribution in oxide superconductors by precise measurements of structure factors

Lijun Wu, Yimei Zhu,* and J. Tafto†

Department of Applied Science, Brookhaven National Laboratory, Upton, New York 11973

(Received 27 May 1998; revised manuscript received 9 October 1998)

We use an approach in electron diffraction, based on quantitative analysis of diffraction intensity of many reflections as a function of sample thickness, to determine Fourier components of the electron distribution in crystals. For short reciprocal vectors our measured accuracy of the Fourier components is, to our knowledge, far beyond previous achievements. This technique is used to study charge transfer and electron-hole distributions in the high-temperature superconductors $\text{Bi}_2\text{Sr}_2\text{CaCu}_2\text{O}_{8+\delta}$ and $\text{YBa}_2\text{Cu}_3\text{O}_7$. Our experimental results agree well with electronic structure calculations. [S0163-1829(99)02210-9]

A great challenge in the studies of condensed matter is to measure the redistribution of electrons that takes place when atoms assemble to form solids, and a good approximation is that only valence electrons are rearranged. Thus, if the x-ray structure factors are known, the valence electron distribution can, in principle, be determined directly by Fourier transform: $\Delta\rho = \rho_m - \rho_a = \sum (F_{gm} - F_{ga}) \exp 2\pi i \mathbf{g} \cdot \mathbf{r}$. Here, the subindex m refers to the ideally measured values of the structure factors F_g and of the electron density $\rho(r)$ in the crystal, and a refers to the corresponding calculated values assuming unperturbed atoms. However, the extraction of sensible information about the valence-electron distribution requires, in addition to extremely accurate measurements of the amplitudes of the x-ray structure factors, also knowledge of their phases that are generally inaccessible from kinematical diffraction experiments. Electron diffraction of fast electrons offers a means of extracting the phases of the structure factors because of the strong dynamical coupling between different beams. Furthermore, in electron diffraction, those structure factors of reflections at small scattering angles that are present for large unit-cell crystals are strongly influenced by the distribution of the valence electrons in the crystal. These advantages of electron diffraction^{1,2} have regained attention in the last few years,³⁻⁷ and it was shown in a recent paper⁶ that a picture of the charge distribution based on an ionic model, with minor adjustments, fits the electron diffraction data of MgO very well. With a recently invented technique of electron diffraction based on simultaneously forming shadow images and thickness fringes of many reflections,^{4,7} we can now accurately determine phases and amplitudes of reflections at small scattering angles in complex crystals. By using this technique, we here address charge transfer and distribution of electron holes in the superconductor $\text{YBa}_2\text{Cu}_3\text{O}_7$ and in the structurally more complicated one $\text{Bi}_2\text{Sr}_2\text{CaCu}_2\text{O}_{8+\delta}$ ($0.12 \leq \delta \leq 0.15$). For these complex crystals neutron and x-ray diffraction have previously been used indirectly to determine the electron-hole distribution in the CuO_2 planes by using empirical bond valence considerations⁸ on accurate data of interatomic distances and coordination numbers. The valency of the different ions has also been addressed directly by x-ray diffraction.⁹ The electron holes play a central role in high-temperature superconductivity because they are the charge carriers in these important materials. We focus on the charge modulation along the

c axis in these complex crystals, and compare our findings with published electronic structure calculations.

Along the c axis, of length 3.08 nm, $\text{Bi}_2\text{Sr}_2\text{CaCu}_2\text{O}_{8+\delta}$ consists of the sequence of layers indicated in Fig. 1 of period $c/2$, resulting in the reflections $002n+1$ being extin-

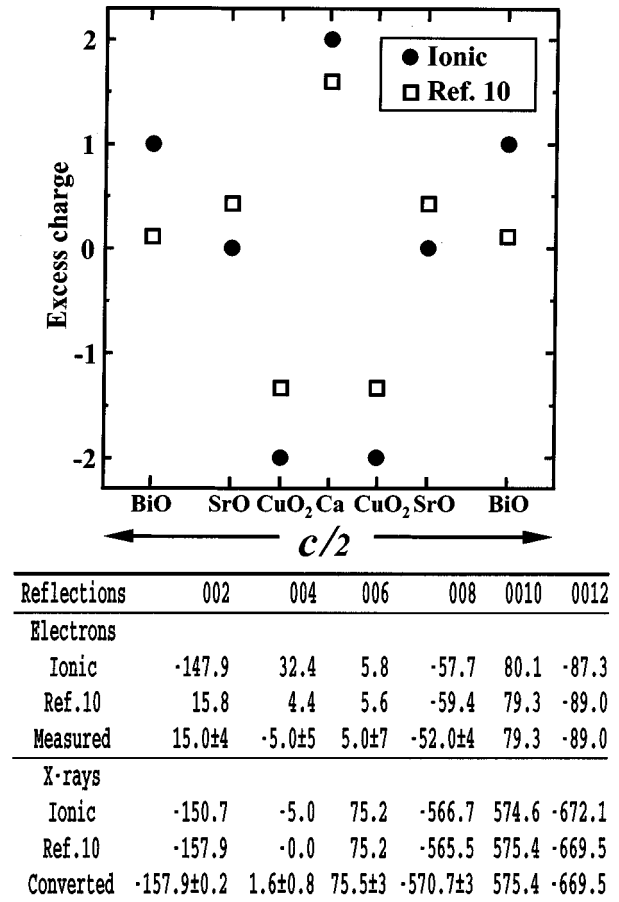


FIG. 1. Charge at the different atomic planes along the c axis of $\text{Bi}_2\text{Sr}_2\text{CaCu}_2\text{O}_{8+\delta}$ in the ionic model and assigned from electronic structure calculations.¹⁰ The sequence of atomic planes is indicated along the horizontal axis. Also shown are the structure factors for electron diffraction and x-ray diffraction calculated assuming a purely ionic model and using the charge assignment of Ref. 10, and as measured and converted from the present electron-diffraction experiments.

guished. With origin chosen at the Ca atom, Fig. 1 also shows calculated structure factors for electron and x-ray diffraction for two different models of the charge distribution; ions of formal valence, i.e., Bi^{3+} , Sr^{2+} , Cu^{2+} , Ca^{2+} and O^{2-} , and a charge distribution determined by electronic structure calculations.¹⁰ We used atomic positions that were determined by a combination of x-ray and neutron diffraction,¹¹ and the scattering amplitudes for x-ray diffraction from the International Tables of Crystallography¹² for most atoms and ions, but for O^{2-} we used Ref. 13. We converted these amplitudes to scattering amplitudes for electrons by the Mott formula: $f_e \sim (Z - f_x)\lambda^2/\sin^2 \theta$. The calculated values of the structure factors in Fig. 1 illustrate the great sensitivity of electron diffraction to charge distribution for the low index reflections. The values of the structure factors of the 002 and 004 reflection change drastically in going from a purely ionic model to the model based on the electronic structure calculation.¹⁰ On the other hand, structure factors of reflections farther out in reciprocal space are only modestly influenced by the valence-electron distribution.

Whereas conventional convergent beam electron diffraction uses ~ 1 nm probe focusing on the sample, our technique to determine structure factors focuses the electron probe above a thin wedge of crystal so that an area of diameter 100 nm or more is illuminated [Fig. 2(a)]. In our technique, the current density is reduced by at least four orders of magnitude, thus minimizing electron-beam damage while acquiring structural information from various thicknesses. A diffraction disc recorded using this technique is demonstrated for Si in Fig. 2(b). The horizontal scan in Fig. 2(b) represents the intensity variation with incident-beam direction, as in a conventional convergent beam diffraction pattern; the vertical scan shows the variation with specimen thickness. In the present study, we had to use a relatively small convergent beam angle to avoid overlap of the closely spaced reflections, thus limiting the information with incident-beam direction. However, with the crossover above the specimen, we can still observe intensity oscillations as a function of specimen thickness, and, more importantly, such oscillations can be observed simultaneously for many reflections in crystals with large unit cells.^{4,7}

High quality wedge crystals were prepared using a wedge polishing technique with the tripod polisher developed by South Bay, Inc. Figures 2(c)–(e) show diffraction patterns with the crossover of the electron probe at increasing distances from the specimen of $\text{Bi}_2\text{Sr}_2\text{CaCu}_2\text{O}_{8+\delta}$. Dynamical Bloch wave calculations were done by including 51 beams. Adjustable experimental parameters were the thickness range, the incident beam direction, and an absorption parameter. Since the areas were thin we used the same absorption parameter for all Bloch waves.

We now compare our observations of $\text{Bi}_2\text{Sr}_2\text{CaCu}_2\text{O}_{8+\delta}$ with different models of the charge modulation, starting with thin region ranging from 0 to 6 nm represented by Fig. 2(c). A scan of this diffraction pattern after subtracting the background around the strong beam in the forward direction is shown in Fig. 3(a) (note the thickness increases from left to right within the discs). The calculated diffraction patterns, convoluted with a Gaussian beam spread function, are shown in Figs. 3(b) and 2(c). The agreement with the observations

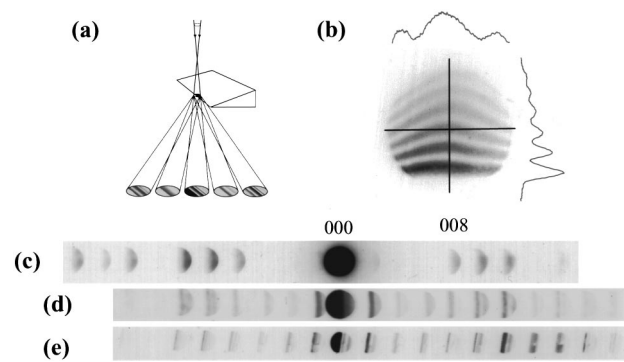


FIG. 2. (a) Schematics of the electron-diffraction technique. (b) A 220 diffraction disc from Si with the crossover above the specimen. The horizontal scan of the 220 disc corresponds to a rocking curve and a vertical scan to thickness fringes. (c), (d), and (e) are diffraction patterns of the 00 l reciprocal lattice row of $\text{Bi}_2\text{Sr}_2\text{CaCu}_2\text{O}_{8+\delta}$ for different thickness ranges of: (c) 0–6 nm, (d) 0–60 nm, and (e) 0–150 nm.

of Fig. 3(a) is reasonable for the model based on electronic structure calculations,¹⁰ Fig. 3(b), whereas the purely ionic model, Fig. 3(c), can be ruled out because the intensity of the 002 reflection is far too high. We now move to the larger thickness range of Fig. 3(d), which is a scan of Fig. 2(d) spanning the thickness from 0 to 60 nm. Calculations based on Ref. 10 gave a good fit. After a small adjustment to the model by moving 0.144 electron from the SrO layer to the BiO layer and 0.056 electrons from the SrO layer to the CuO layer per unit cell, the calculated structure factors become consistent with the experimentally measured values. To evaluate the goodness of fit and estimate the error range of the measurement, we modified the R factor traditionally used in crystallography.¹⁴ $R = (\sum_{g_i, t_j} |I_{obs} - I_{cal}| / \sum_{g_i, t_j} |I_{obs}|) \times 100$, where g_i ($i = 1, 2, \dots$) is a reciprocal vector and t_j ($j = 1, 2, \dots, 50$) represents the partition of the thickness. We note that our R factor is much more demanding than the traditional one that considers only a constant thickness. Here, we take into account the variation of the intensity profile with thickness for the different reflections. The R values for Figs. 3(b) and (c) are 15.2 and 38.8, respectively. These R values must be judged on the fact that for this dense reciprocal row the dynamical coupling between the reflections is very strong. Thus, small changes in the values of the structure factors drastically alter the intensity of the reflections with increasing thickness. In most situations, our R factor is below 0.01 in thin areas of maximum thickness less than 5 nm where the scattering is close to kinematical. The R factor may exceed 0.5 for a thickness larger than 100 nm due to the strong dynamical coupling between the reflections. The R value can be significantly reduced for thick crystals if we integrate over the whole range of thicknesses, similar to the case of x-ray diffraction, i.e., considering R is a function of g only, rather than g and t . Through quantitative refinement, Fig. 3(e) we concluded that for $\text{Bi}_2\text{Sr}_2\text{CaCu}_2\text{O}_8$ the value of the structure factor of the 002 and 004 reflections are $+15 \pm 4 \text{ \AA}$ and $-5 \pm 5 \text{ \AA}$ which, after conversion to x-ray structure factors, are -157.9 ± 0.2 electrons and 1.6 ± 0.8 electrons, respectively.

A somewhat simpler system than $\text{Bi}_2\text{Sr}_2\text{CaCu}_2\text{O}_{8+\delta}$ is the $\text{YBa}_2\text{Cu}_3\text{O}_7$ superconductor.⁴ Figure 4(a) shows scan of a

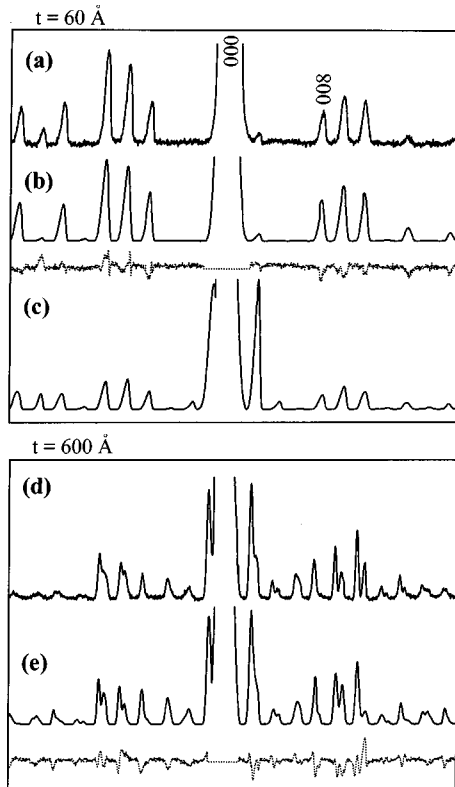
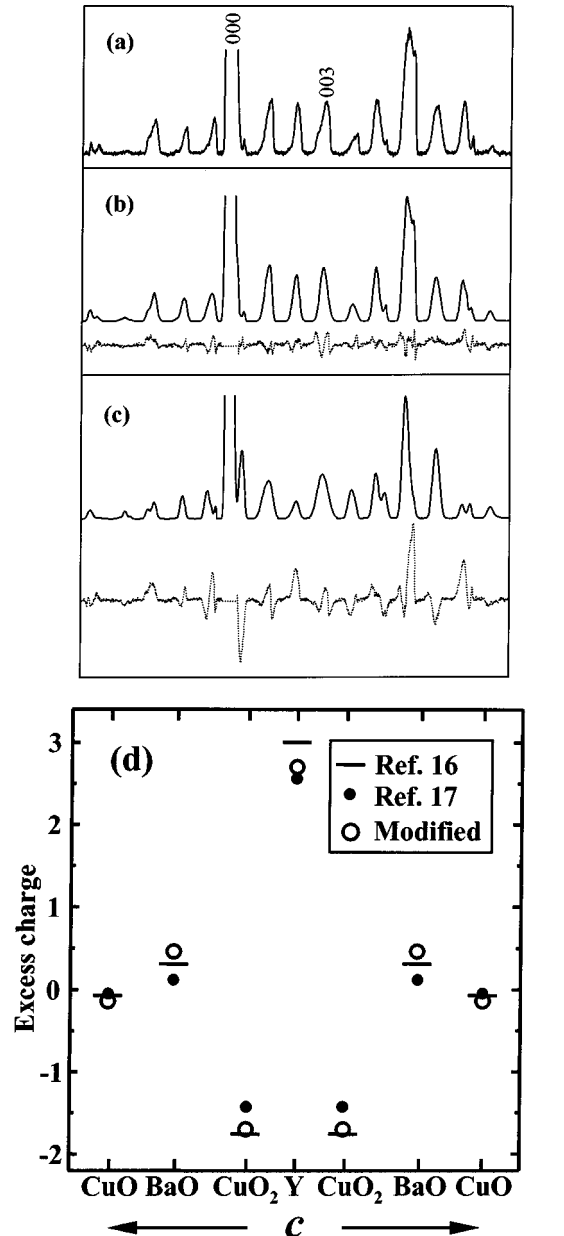


FIG. 3. (a) Scan of the intensity profile of the diffraction pattern of Fig. 2(c). Note the 00-2 peak is shadowed due to overlap with the high intensity outside the specimen in the 000 disc. (b) and (c) are calculated profiles for two models of the charge modulations: (b) Ref. 10; (c) purely ionic. (d) Scans of the intensity profile of the diffraction pattern of Fig. 2(d). (e) Calculated intensity profile with the best fit of the 002 and 004 structure factors. The difference (dotted line) between the observations and calculations for (b) and (e) also are included. The center of the Laue circle is at 00-17 for (a), and 001 for (d).

diffraction pattern of the 001 reciprocal lattice row. Using crystallographic data from Ref. 15 and origin chosen at the CuO plane, we obtained the smallest R value of 16.8, Fig. 4(b), by adjusting the scattering amplitude of the 001 and 002 structure factors to the values $-3.4 \pm 0.9 \text{ \AA}$ and $-4.0 \pm 1.1 \text{ \AA}$, respectively. These accuracies in electron diffraction correspond to accuracies of the x-ray structure factors of 0.1 and 0.4 electron, respectively. By using the charge assigned to the atoms from electronic structure calculations,^{16,17} the agreement with experiment was poor, as shown for the model of Ref. 17 in Fig. 4(c) with an R value of 40.2. However, the sensitivity of electron diffraction at these low angles is so high that by the small changes relative to these models indicated in Fig. 4(d), the calculated diffraction patterns approached the experimental ones. Relative to the model of Ref. 16, this modification amounts to moving per unit cell 0.3 electrons from the BaO layer to the Y layer, and 0.05 electrons from the CuO_2 layer to the CuO layer.

The structure factors of the low-order reflections could be brought within acceptable range of the experimentally determined values by extremely small adjustments to the models. For $\text{YBa}_2\text{Cu}_3\text{O}_7$ Brown⁸ concludes using bond valence considerations on the crystallographic data from neutron diffraction¹⁵ that we use in this study, that there are 0.3 elec-



Reflections	001	002	003	004	005	006
Electrons						
Ref.17	-9.1	-2.0	-10.4	-3.5	16.6	21.3
Measured	-3.4 ± 0.9	-4.0 ± 1.1	-11.2 ± 0.9	-4.5 ± 1.0	16.6	21.3
X-rays						
Ref.17	-6.6	-18.5	-41.9	-22.5	102.3	150.9

FIG. 4. (a) Intensity scan from a diffraction patterns of $\text{YBa}_2\text{Cu}_3\text{O}_7$ with thickness ranging from 0–50.0 nm (the center of the Laue circle is at 003). (b) Best fit to the observations, together with its difference (dotted line). (c) Calculations using the model of Ref. 17. (d) Charge distribution in different models. The open circles are for the modification described in the text that gave an intensity profile in fair agreement with the observations. Also shown are the structure factors for electron diffraction and x-ray diffraction as calculated using the charge assignment of Ref. 17, and measured experimentally from the present work.

tron holes per CuO_2 unit in the CuO_2 planes. The electronic structure calculations^{16,17} suggest 0.24 and 0.28 holes, respectively, and our experimental study suggests 0.25 electron holes per CuO_2 unit.

To summarize, we have shown that electron diffraction can be used to study the small changes in the electron distribution, and this can be done even in complex crystals containing atoms of high atomic numbers, such as the high-temperature superconductors with a high density of core electrons. For example, the movement of 0.05 electron holes per the unit cell of $\text{YBa}_2\text{Cu}_3\text{O}_7$ between the CuO chain and

the CuO_2 plane that corresponds to rearranging 1 out of 5000 electrons in the crystal, changes the 001 structure factor of electron diffraction by 1 Å while we determine this structure factor with an accuracy of 0.9 Å. With this great sensitivity, we feel confident that the technique which we developed to study structure factors and valence-electron distribution of $\text{Bi}_2\text{Sr}_2\text{CaCu}_2\text{O}_{8+\delta}$ and $\text{YBa}_2\text{Cu}_3\text{O}_7$, will become a rather general procedure for precision studies of complex crystals.

The research was supported by the U.S. Department of Energy, Division of Materials, Office of Basic Energy Science, under Contract No. DE-AC02-98CH10886.

*Corresponding author; electronic address: zhu@bnl.gov

†Visiting scientist from Dept. of Physics, Univ. of Oslo, Norway.

¹J. M. Cowley, *Acta Crystallogr.* **6**, 516 (1953).

²G. R. Anstis, D. F. Lynch, A. F. Moodie, and M. A. O'Keefe, *Acta Crystallogr., Sect. A: Cryst. Phys., Diffr., Theor. Gen. Crystallogr.* **A29**, 138 (1973).

³J. M. Zuo, J. C. H. Spence, and R. Hoier, *Phys. Rev. Lett.* **62**, 547 (1989).

⁴Y. Zhu and J. Taftø, *Philos. Mag. B* **75**, 785 (1997).

⁵Y. Zhu and J. Taftø, *Phys. Rev. Lett.* **76**, 443 (1996).

⁶J. M. Zuo, M. O'Keefe, and J. C. H. Spence, *Phys. Rev. Lett.* **78**, 4777 (1997).

⁷J. Taftø, Y. Zhu, and L. Wu, *Acta Crystallogr., Sect. A: Found. Crystallogr.* **A54**, 532 (1998).

⁸I. D. Brown, *J. Solid State Chem.* **90**, 155 (1991).

⁹S. Sasaki, Z. Inoue, N. Iyi, and S. Takekawa, *Acta Crystallogr., Sect. B: Struct. Sci.* **B48**, 393 (1992).

¹⁰R. P. Gupta and M. Gupta, *Phys. Rev. B* **49**, 13 154 (1994).

¹¹Y. Gao, P. Coppens, D. E. Cox, and A. R. Moodenbaugh, *Acta Crystallogr., Sect. A: Found. Crystallogr.* **A49**, 141 (1993).

¹²*International Tables of Crystallography* (Kluwer Academic, Dordrecht 1992), Vol. C, p. 475.

¹³D. Rez, P. Rez, and I. Grant, *Acta Crystallogr., Sect. A: Found. Crystallogr.* **A50**, 481 (1994).

¹⁴H. M. Rietveld, *J. Appl. Crystallogr.* **2**, 65 (1969).

¹⁵J. D. Jorgensen, B. W. Veal, A. P. Paulikas, L. J. Nowicki, G. W. Crabtree, H. Claus, and W. K. Kwok, *Phys. Rev. B* **41**, 1863 (1990).

¹⁶W. E. Pickett, *Rev. Mod. Phys.* **61**, 433 (1989).

¹⁷R. P. Gupta and M. Gupta, *Phys. Rev. B* **44**, 2739 (1991).